Aluminum doped core-shell ZnO/ZnS nanowires: Doping and shell layer induced modification on structural and photoluminescence properties

Soumen, Dhara
Imakita, Kenji
P. K. Giri
Mizuhata, Minoru
Fujii, Minoru

(Citation)
Journal of Applied Physics,114:134307-134307

(Issue Date)
2013

(Resource Type)
journal article

(Version)
Version of Record

(URL)
https://hdl.handle.net/20.500.14094/90002571

Aluminum doped core-shell ZnO/ZnS nanowires: Doping and shell layer induced modification on structural and photoluminescence properties

Soumen Dhara, Kenji Imakita, P. K. Giri, Minoru Mizuhata, and Minoru Fujii

Citation: Journal of Applied Physics **114**, 134307 (2013); doi: 10.1063/1.4824288
View online: http://dx.doi.org/10.1063/1.4824288
View Table of Contents: http://scitation.aip.org/content/aip/journal/jap/114/13?ver=pdfcov
Published by the AIP Publishing

Aluminum doped core-shell ZnO/ZnS nanowires: Doping and shell layer induced modification on structural and photoluminescence properties

Soumen Dhara,[1,a)] Kenji Imakita,[1] P. K. Giri,[1,2] Minoru Mizuhata,[3] and Minoru Fujii[1,a)]
[1]*Department of Electrical and Electronic Engineering, Faculty of Engineering, Kobe University, 1-1 Rokkodai, Nada, Kobe 657-8501, Japan*
[2]*Department of Physics, Indian Institute of Technology Guwahati, Guwahati 781 039, India*
[3]*Department of Chemical Science and Engineering, Faculty of Engineering, Kobe University, 1-1 Rokkodai, Nada, Kobe 657-8501, Japan*

(Received 20 August 2013; accepted 18 September 2013; published online 2 October 2013)

In this work, we investigated the combined effects of Al doping and surface modification on the fabrication of a core–shell type ZnO/ZnS nanowires (NWs) and its structural, electrical, and photoluminescence (PL) properties. A systematic investigation for different concentrations of Al doping followed by surface modification with different thicknesses of ZnS layer was performed. Significant changes in the nature of PL spectra and electronic conductivity are observed and insight discussions are present. Structural characterization on the core-shell NWs reveals the successful fabrication of Al doped highly single crystalline ZnO core and polycrystalline ZnS shell with both ZnO and ZnS are of hexagonal wurtzite structure. Compared with the bare undoped ZnO NWs, Al doped core-shell ZnO/ZnS NWs exhibit two orders of magnitude improvement in the electronic conductivity and fivefold enhancement in the UV PL intensity. The Al doped core-shell ZnO/ZnS NWs shows an efficient improvement in the UV PL intensity than the undoped core-shell ZnO NWs. The obtained improvement in the PL result is explained on the basis of interfacial transfer of photogenerated charge carriers and modification of defects. © *2013 AIP Publishing LLC*. [http://dx.doi.org/10.1063/1.4824288]

I. INTRODUCTION

ZnO, a versatile material with several important properties, e.g., strong room temperature UV photoluminescence (PL), high transparency in the visible region, piezoelectric, ferromagnetic, nonlinear optical properties, etc., has attracted the attention of the researchers worldwide. These interesting features of ZnO enables to fabricate various nanodevices ranging from field effect transistors to biosensors using various types of ZnO nanostructures.[1–4] ZnO nanowires (NWs) are extensively studied for the ease of the devices fabrication process and have the ability to be integrated into the mainstream Si based electronics for future large-scale optoelectronic device integration.[5,6] However, successful commercial application of ZnO NWs based devices requires detail understanding and control over the growth of the ZnO NWs, structural quality, and specific properties related to the application purpose. Depending upon the growth method, the as-grown ZnO NWs invariably contain several surface defects which have a detrimental effect on the band edge UV emission and related applications.[7] Hence, obtaining highly efficient UV emission from the ZnO nanostructures is one of most important issues for optoelectronic applications of ZnO. Furthermore, the electronic conductivity of the as-grown ZnO NWs is usually low for device application. The electrical, optical, and magnetic properties of ZnO can be adjusted desirably not only by impurity doping but also through surface modification.[8–13] The modification of the surface is considered as one of the advanced techniques to change the physical properties of ZnO for a better nanoscale application.[14–16] In this context, researchers fabricated various types of hybrid or heterostructures with some suitable external material. Here, the external material significantly influences the specific properties of the core material. In our previous reports, we demonstrated the use of anthracene and copper pthalocyanine (CuPc) for the fabrication of ZnO/organic NWs heterostructure.[17,18] We observed a notable improvement in the UV PL and photoresponse properties and it was explained on the basis of photo-induced interfacial charge transfer process. It is also noticed that the photosensitivity of the external material and the structural quality of the interface strongly control the properties of the heterostructures. Therefore, it is very important to devote an in-detail study about the structure and other properties of a NW heterostructure with a new external material for better control and understanding. There are few reports on the fabrication of ZnO NW heterostructure with ZnS as a shell layer. Panda *et al.*[19] prepared ZnO-ZnS core-shell nanorods by partial conversion of the ZnO nanorod surface to ZnS at 400 °C under H_2S and argon gas mixture and studied the luminescent properties. Liu *et al.*[20] reported the enhancement of photocurrent conversion efficiency by using ZnO/ZnS nanorods as the photoanode for a photovoltaic device. Li *et al.*[21] showed the enhancement of UV emission from ZnS-coated ZnO nanowires fabricated by self-assembling method using sodium sulfide and zinc nitrate. Efficient conversion of mechanical energy (by deflection of the NWs) to electrical energy (voltage generation) is also demonstrated by using ZnO-ZnS axial heterojunction NW arrays which were

[a)]Authors to whom correspondence should be addressed. Electronic addresses: fujii@eedept.kobe-u.ac.jp and soumen5484@yahoo.co.in

synthesized by thermal evaporation process.[22] However, the combined effect of doping and a shell layer on the resulting optoelectronic properties of ZnO NWs has not been studied systematically.

In this work, we employ Al doping in ZnO NWs followed by surface modification with a ZnS shell layer to investigate the doping and shell layer induced modification on the ZnO NWs. The as-prepared Al doped ZnO NWs have sufficiently higher electronic conductivity. However, the UV emission is not sufficiently strong for optoelectronic applications in large scale commercial purpose. To improve further, ZnS was chosen as a shell layer due to the higher bandgap energy and semiconducting nature of the ZnS, it is expected that outer shell layer will influenced to get an improvement in UV PL. A detailed investigations on structural and PL properties were performed by preparing a set of samples with different concentrations of Al doping and with various thicknesses of outer ZnS shell layer.

II. EXPERIMENTAL

ZnO NWs were grown by an aqueous chemical growth method as described elsewhere.[23] In brief, uniform distribution of ZnO nanocrystal seeds were prepared on a Si substrate by spin coating followed by thermal decomposition of a zinc acetate precursor. Coating process was repeated several times for 30 s each to get sufficient thickness of the zinc acetate layer. Then the coated substrate was heated at 350 °C for 30 min to get ZnO seed layer. The vertically-aligned ZnO NWs were synthesized by hydrolysis of zinc nitrate (Wako Chem.) in water in presence of hexamethylenetetramine (HMT, Wako Chem.) on the above prepared substrate. For Al doping, aluminum nitrate was used as precursor solution which was mixed properly in the reaction solvent according to the stoichiometric ratio. An equimolar (25 mM) concentration of zinc nitrate, aluminum nitrate, and HMT in DI-water and polyethyleneimine (9 mM) were mixed properly in a Teflon made reaction flask. The above prepared substrate was dipped in to the reaction solvent mixture and placed vertically. Then the reaction flask was sealed inside an autoclave. The chemical reaction was carried out at 95 °C for 24 h in the autoclave. The substrate was then removed from the solution, rinsed in DI-water and dried in hot air at 100 °C for 30 min. In this process, 0.5, 1.0, 2.0, and 5.0 at. % of Al doped ZnO (Al:ZnO) NWs were prepared. For comparison, undoped ZnO NWs were prepared by the same process without using doping precursor solution.

For the ZnS shell preparation, the previously prepared Al(2 at. %):ZnO NWs were dipped into 10 mM aqueous solution of thioacetamide (TAA, Wako Chem.) at 60 °C for 1, 2, and 4 h and then dried. In this process, we prepared core-shell type ZnO/ZnS NWs with varying thickness of ZnS shell layer. Samples are marked as CS1, CS2, and CS4 for the sulfidization time duration of 1, 2, and 4 h, respectively. For comparative studies, above mentioned sulfidization process was repeated for undoped ZnO NWs for 2 h. Field emission scanning electron microscopy (FESEM, JSM6335F, JEOL) was used to confirm the formation of ZnO NWs. The crystal structure (structural analysis) of the above prepared NWs was characterized using x-ray diffraction (XRD, Ultima IV, Rigaku) and transmission electron microscopy (TEM, JEM2010, JEOL) operated at 200 keV with selected area electron diffraction (SAED). To trace the elemental composition in the as grown NWs, energy dispersive x-ray spectroscopy (EDX) and x-ray photoelectron spectroscopy (XPS) were employed. XPS measurement was carried out with a fully automated XPS microprobe (Phi-χtool, Ulvac-Phi) using Al K_α x-ray beam (1486.7 eV) with beam current of 5 mA. Carbon 1s spectrum was used for the calibration of the XPS spectra recorded for various samples. The room temperature PL spectra of all the samples were recorded with a 325 nm He–Cd laser excitation using a commercial PL spectrometer (Flurolog-3, Horiba) equipped with a PMT (photo multiplier tube) detector. For comparative analysis, PL measurements on all the samples were made under identical experimental conditions.

III. RESULTS AND DISCUSSION

A. Structural studies

Figure 1(a) shows the FESEM morphology image of the undoped ZnO NWs grown by an aqueous chemical method with the help of ZnO seed layer. As seen in the image, high density ZnO NWs grow vertically on the Si substrate over a large surface area with NWs density of 3.2×10^{13} cm^{-2}. Figures 1(b) and 1(c) show the tilted view of the undoped and Al(1 at. %):ZnO NWs. The diameters of the NWs are very small, which ranges from 35 to 60 nm for the undoped one and from 40 to 60 nm for the Al(1 at. %):ZnO NWs and the lengths are about a few microns. The Al:ZnO NWs with different concentrations of Al show similar morphology with varying diameter. From the morphology studies, it is seen that degree of alignment of the NWs goes down with the increase in Al doping concentration. During the chemical growth process, ZnO NWs preferentially nucleate from the tip near the grain boundaries between two adjacent grains in

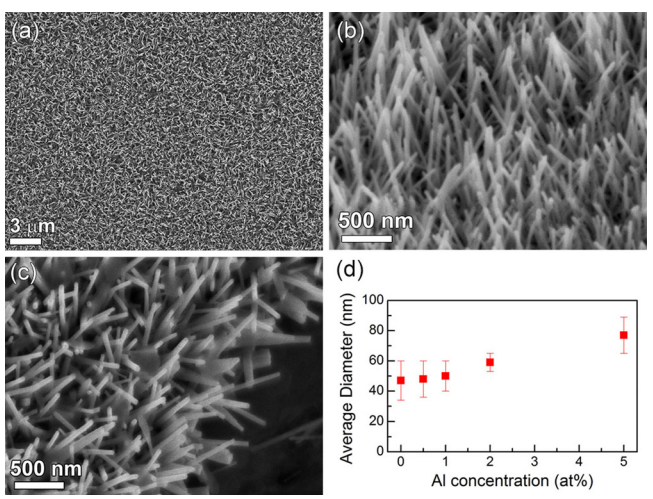

FIG. 1. (a) FESEM image (top view) of the chemically grown undoped ZnO NWs. (b) and (c) Magnified tilted view image of the above ZnO NWs and Al doped Al(1 at. %):ZnO NWs, respectively. (d) Diameter variation of the chemically grown undoped and Al doped ZnO NWs as a function of Al concentration.

the ZnO seed film.[24] The degree of alignment in the as-grown ZnO NWs is strongly controlled by the orientation of the ZnO seed layer. During growth process, the doping of Al atoms inside the ZnO lattice may cause lattice distortion, which affects the initial growth orientation. Figure 1(d) shows the diameter variation of the Al:ZnO NWs as a function of Al doping concentration. The Al doping slowly increases the diameter of the NWs and it is saturated at higher concentration of Al (more than 5 at. %, data not shown). Whereas the Al doping has no significant influence on the length of the NWs, as expected. It is known that the diameter of the as-grown NWs usually depends on the grain size of the ZnO seeds and the reaction process, while the length of the NW primarily controls by the reaction time duration.

Figure 2(a) shows FESEM image of the bare Al(2 at. %):ZnO NWs and Fig. 2(b) shows the core-shell type Al(2 at. %):ZnO NWs with ZnS shell. The Al doping in the as-prepared NWs was confirmed from the corresponding EDX spectrum. The EDX spectrum of the Al(2 at. %):ZnO NWs in Fig. 2(c) shows the presence of 1.46 at. % of Al atoms. From the EDX elemental analysis, it is found that the Al doping concentration is lower than those in the mixed reaction solutions. This inadequacy increases with the increase in Al concentration in the mixed reaction solution. In the case of chemical doping at higher dopant concentration, the Al atoms might be nucleated with hydroxyl ions present in the growth solution due to the kinetic equilibrium. Thus, it would be difficult for all of the Al^{3+} ions to be incorporated into ZnO lattice at higher concentration, similar to the case of Mn doping.[25] In the case of Al doping, majority of the Al atoms occupy the ZnO lattice by substitution of Zn atoms. However, there is also a possibility of formation of interstitial Al atoms in the ZnO lattice due to its smaller size than the Zn atoms. EDX analysis further shows that the oxygen content is slightly higher than Zn content, although oxygen vacancies are usually present on the NWs surface. The extra oxygen in the EDX spectrum may arise from the hydroxyl radicals (-OH groups) present on the surface of the ZnO NWs. The FTIR data of the undoped ZnO NWs shown as inset in the Fig. 2(c) confirm the existence of sufficient amount of hydroxyl radicals on the surface of the NWs. We also observed stretching and bending vibration mode of Zn-O bonds in the FTIR spectrum. Presence of hydroxyl radicals (−OH groups) is further, confirms, from the XPS and PL spectroscopic data (explained later).

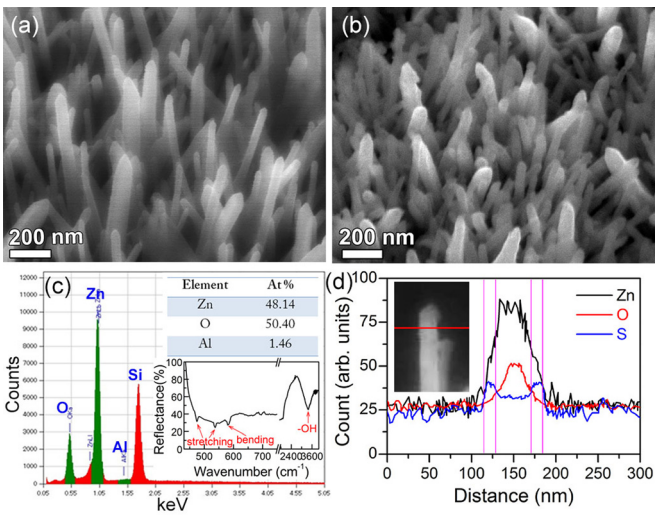

FIG. 2. (Tilted view) FESEM images of the chemically grown ZnO NWs: (a) Al(2 at. %):ZnO and (b) sample CS4. (c) EDX spectrum of the above Al(2 at. %):ZnO NWs. Inset shows the FTIR reflectance data of the undoped ZnO NWs. (d) EDX line scan across the diameter of a single core-shell NW of sample CS4.

After the sulfidization process, a clear difference in the surface morphology of the bare Al(2 at. %):ZnO and sample CS4 NWs can be visualized from the images as the sidewalls of the former are smooth, whereas those of the latter are rough and wrinkled indicating some modification has been occurred on the surface due to ZnS layer formation. The CS1 and CS2 show similar surface morphology with relatively smoother sidewall than the case of CS4. There is no significant change in the diameter of the core-shell NWs indicating that only the surface of the ZnO layer is converted to ZnS. This is because the conversion of ZnO to ZnS is essentially a substitution reaction,[26] and only growth of the ZnS shell takes place. To confirm the formation of outer ZnS shell layer further, EDX elemental line scan technique is employed across the diameter of a single core-shell NW, which is shown in Fig. 2(d). This profile illustrated the presence of higher O concentration in the central region and higher S concentrations at both edge regions of the NW. It confirms the successful formation of interface between the Al:ZnO core and ZnS shell. The estimated core diameter is ~41 nm and shell thickness is ~14 nm for the sample CS4.

The structural analysis of the undoped, Al doped, and doped core-shell ZnO NWs is performed from the TEM and XRD results. Figure 3 shows the typical TEM images of the undoped, Al doped ZnO, and doped core-shell ZnO/ZnS NWs. Diameters and lengths of the NWs measured from the TEM images are consistent with the sizes obtained from the corresponding FESEM images. Figure 3(a) shows the low-resolution TEM image of the undoped ZnO NWs and the corresponding SAED pattern. The SAED pattern indicates the highly crystalline hexagonal structure of the undoped ZnO NWs with zone axis along (001). Figure 3(b) shows the high-resolution lattice image of a single NW which further confirms the highly crystalline structure with growth direction along ⟨001⟩ (c-axis). The lattice spacing is calculated to be 2.6 Å corresponding to the (002) plane of hexagonal structure. Figure 3(c) shows the TEM image of the Al(2 at. %):ZnO NW and its corresponding SAED pattern and lattice image. The doped NWs also possess high crystallinity, as seen from the Fig. 3(c). The successful formation of core-shell structure is further confirmed from the TEM image of the sample CS4 as shown in Fig. 3(d). The contrast difference in the center and at the edges of the NW confirms the core-shell structure with core diameter ~33 nm. The lattice spacing calculated in the centre and at the edge corresponds to the (002) plane of ZnO and (100) plane of ZnS with both have hexagonal structure. It is noticed that the shell layer is not continuously smooth rather it is a formation of polycrystalline grains of ZnS, as seen from the inset image. The measured shell thickness is ~19 nm which is larger than the

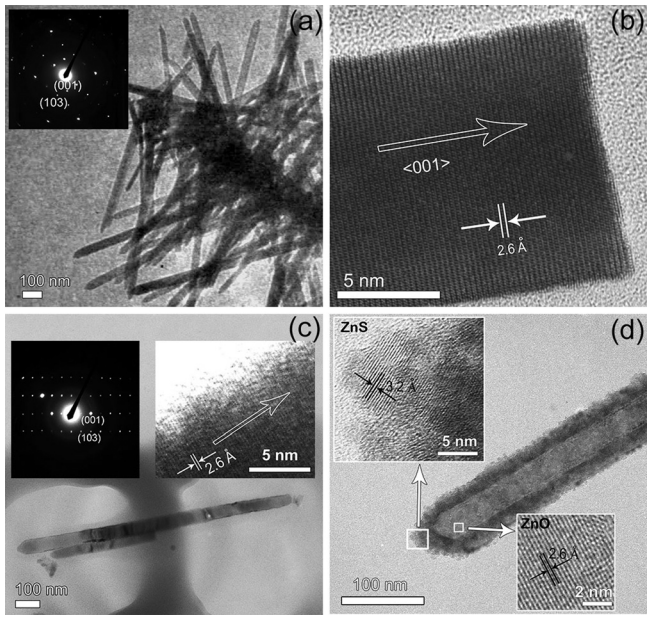

FIG. 3. (a) A typical low-resolution TEM image of the undoped ZnO NWs. (b) High resolution lattice image of the above ZnO NW. Inset in (a) shows the corresponding SAED pattern. (c) and (d) TEM images of the Al doped Al(2 at. %):ZnO and Al(2 at. %):ZnO/ZnS NW (sample CS4), respectively. Inset images in (c) show the corresponding SAED pattern and high-resolution lattice image of the NW. Inset images in (d) show the high-resolution lattice image of the corresponding selected area in the above core-shell NW. Hollow arrow indicates the growth direction of the NW.

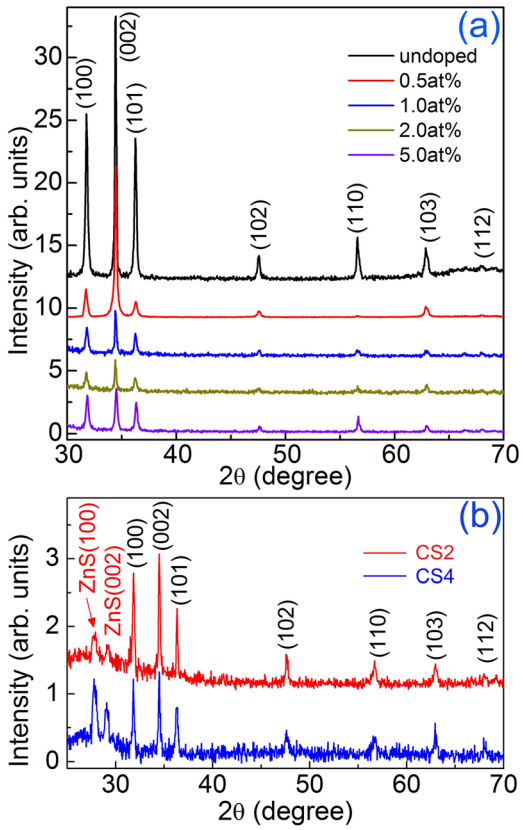

FIG. 4. (a) X-ray diffraction patterns of the chemically prepared undoped and Al doped ZnO NWs with different concentrations of Al doping; (b) X-ray diffraction patterns of the core-shell ZnO/ZnS NWs for varying thickness of the shell layer.

size obtained from the EDX line scan data. The smaller estimation in the EDX data might be due to the very rough sidewall of the ZnO/ZnS NWs. Further structural characterization by XRD measurements shows characteristic peaks of crystalline hexagonal phase of ZnO in the XRD patterns. Comparatively, stronger intensity of the (002) peak (Fig. 4(a)) indicates that the ZnO NWs are aligned along the normal to the substrate plane. No other peaks related to the Al or aluminum oxide are detected. The relative intensity of the strong (002) peak goes down with the increase in Al doping concentration. As compared with the undoped case, the intensity decreases by six fold after 5 at. % of Al doping. This indicates a deterioration of the structural quality with the increasing in Al doping concentration, although the Al(5 at. %):ZnO NWs still have good crystalline nature. Exact position of the (002) peak is calculated from the Lorentzian fitting to the experimental data. It is found that the peak position is slightly shifted towards higher 2θ. This up shift indicates lower lattice spacing and it implies that the Al:ZnO NWs are weakly strained compressively. It is also noticed that the compressive strain increases with increase in Al concentration, as expected. The calculated strain value increases from 0.09% to 0.25% from undoped to Al(5 at. %):ZnO NWs. Similar compressive strain has been reported earlier in the Al doped ZnO thin films.[27] As explained earlier, due to the smaller size of the Al atom than Zn atom, incorporation of Al atoms into ZnO leads to slight decrease in lattice constants in ZnO, resulting in the compressive strain in the Al:ZnO NWs. Figure 4(b) shows the XRD patterns of the core-shell ZnO NWs. The relative intensities of the peaks corresponding to ZnO further reduced due to the formation of outer shell. Additional peaks correspond to the lattice planes of hexagonal phase of ZnS are also observed in the XRD data. It is also noticed that the relative intensities of the ZnS related peak increase for sample CS4. This indicates that in the sample CS4, the ZnO NW has thicker outer shell than the NW in the sample CS2, as expected.

Further information about chemical elemental environment and surface defects of the ZnO NWs is obtained from the XPS analysis. Figure 5 shows the collective binding energy spectra of the elements under analysis for the undoped, Al:ZnO NWs, and sample CS2. Al 2p core level spectrum of undoped ZnO NWs shown in Fig. 5(a) shows no detectable signal in the range 68–80 eV indicating absence of Al as impurity. On the other hand, a significant peak at 74.0 eV is detected from each of the Al:ZnO NWs (Figs. 5(b)–5(d)). The observed peak can be attributed to the binding energy of Al 2p core level doublet. This peak position of Al corresponds to an oxidation state close to Al^{3+} in Al_2O_3 (Al 2p: 75.6 eV)[28] thereby giving further support for Al residing at substitutional positions rather than at interstitial sites in the ZnO crystal. This also ruled out the possibility of presence of Al_2O_3 or segregation of metallic Al (Al 2p: 72.8 eV)[29] on the surface of the Al:ZnO NWs. It is also noticed that the integrated peak area for the Al 2p core level gradually increases with the increase in Al doping concentration, as expected. The Al doping level in the Al:ZnO NWs is further quantify from the integrated peak area of Al 2p, O 1s, and Zn 2p core level XPS peaks. The Al concentration is

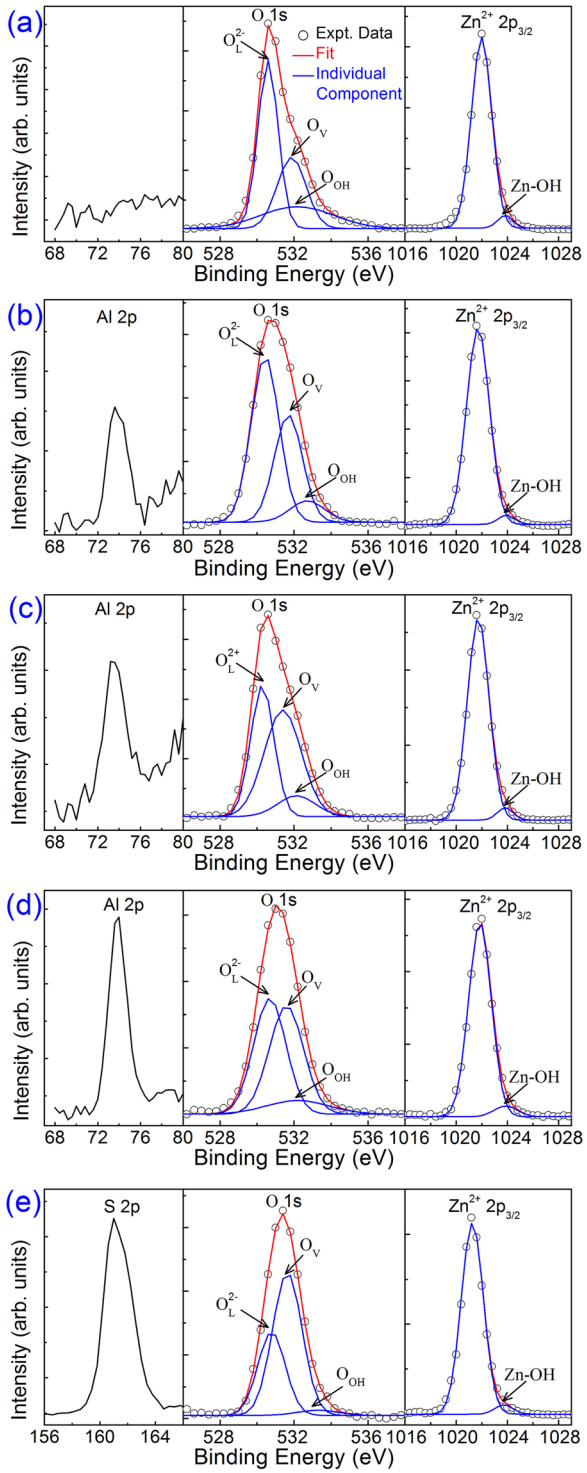

FIG. 5. (a)–(d) XPS binding energy spectra of the undoped, 1 at. %, 2 at. %, 5 at. % of Al doped ZnO NWs, respectively. (e) XPS data of the core-shell CS2 NWs sample. To find the individual components, experimental XPS data (circle) are fitted with multi-Gaussian Peakfit. Solid red line represents the combined fitting of sum of all the individual components (blue line).

estimated according to the standard method (calculation of fractional peak area divided by individual sensitivity factor of each XPS peak). The calculated Al concentrations are found to be close (1.6 at. % for 2% mixed Al in the solution) to the doping concentration in the mixed reaction solution and it is slightly higher than the concentration obtained from the EDX analysis. The XPS spectra for the O 1s and Zn 2p$_{3/2}$ core levels show broad asymmetric nature indicating presence of multi-component species. The O 1s spectrum is deconvoluted to three components centered at 530.6, 531.8, and 532.2 eV. The first peak with lowest binding energy (O_L^{2-}) of the O 1s spectrum can be attributed to the O^{2-} ions in the hexagonal structure of ZnO lattice surrounded by zinc atoms.[30] The intermediate binding energy peak (O_V) is associated with O^{2-} ions that are in oxygen deficient regions within the matrix of ZnO.[30] The higher binding energy peak (O_{OH}) at 532.2 eV usually corresponds to absorbed hydroxyl group (−OH) on the surface (preferable at the oxygen vacancy sites) of the NWs.[31] From the comparative studies, it is found that the integrated peak area for the O_V peak gradually increases with the increase in Al doping concentration. The calculated content of O_V peak in O 1s XPS spectrum changes from 29% to 45% for the undoped to Al(5 at. %):ZnO NWs. This indicates a gradual increasing of defect concentration with the increase in Al doping concentration and it is consistent with the XRD analysis. The XPS data for the Zn 2p$_{3/2}$ core level are also deconvoluted and the peak is best fitted with two symmetric Gaussian peaks. The peak centered at 1021.9 eV is known as Zn 2p$_{3/2}$ spectral line for Zn^{2+} in ZnO lattice. Along with the Zn 2p$_{3/2}$ peak, another peak at 1045.2 eV corresponds to the Zn 2p$_{1/2}$ observed in the XPS spectra (data not shown). The second peak centered at 1023.8 eV can be attributed to the zinc complex with adsorbed hydroxyl group (Zn-OH).[32] From the CS2 sample (Fig. 5(e)), along with the O 1s and Zn 2p core level, sufficient amount of signal is obtained for the S 2p core level in ZnS lattice. After the formation of outer ZnS shell layer, the defect concentration significantly enhanced to 62.8% of O 1s XPS spectrum, as expected. During sulfidization process, the S atoms in TAA solution replace the O atoms in the ZnO lattice. Due to the uncontrolled rate of sulfidization process, oxygen vacancy concentration is likely to increase.

B. Electrical studies

The electrical characterization is performed on the undoped and Al:ZnO NWs. The resistivity of the NWs is estimated from the current-voltage data measured by standard four-probe setup. It is found that the electronic conductivity gradually increases with the increase in the Al concentration in the NWs. The undoped ZnO NWs show low electronic conductivity with a resistivity of ~46.8 Ω cm. Al doping causes dramatic improvement in conductivity of the ZnO NWs. The conductivity improved by two orders of magnitude for the Al(5 at. %):ZnO NWs with the lowest resistivity of ~0.45 Ω cm. The obtained high conductivity is the result of activation of large numbers of Al dopants in the ZnO lattice.

C. Photoluminescence studies

The room temperature PL spectra of the undoped and Al:ZnO NWs are shown in Figs. 6(a)–6(e). The ZnO NWs exhibit near band edge (NBE) UV emission at ~380 nm and a broad visible emission band in the green–yellow region. Deconvolution of this broad emission by Gaussian multipeak fitting shows the existence of two emission bands, one at

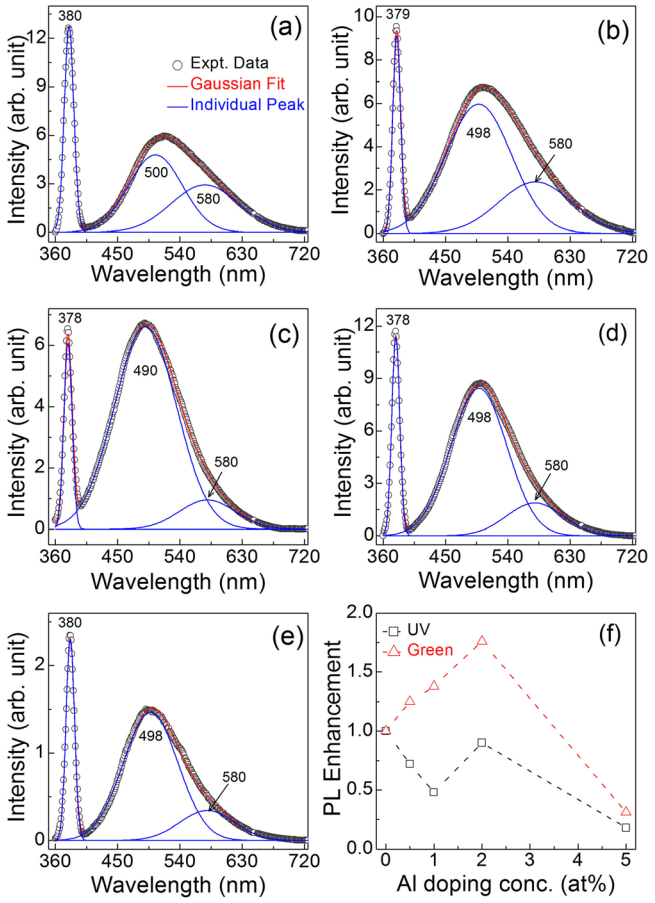

FIG. 6. Room temperature PL spectra of the (a) undoped and Al doped ZnO NWs for Al doping concentration of (b) 0.5 at. %; (c) 1 at. %; (d) 2 at. %, and (e) 5 at. %. (f) Variations of PL enhancement (intensity ratio) of UV and green emissions with respect to undoped ZnO NWs as a function of Al doping concentration. Dotted lines are shown as a viewing guidance to the data points. To find the individual PL peak, experimental data (circle) are fitted with multi-Gaussian Peakfit. Solid red line represents the combined fitting of sum of all the individual components (blue line).

green region (~500 nm) and another at yellow region (580 nm). The observed NBE emission is due to free excitonic recombination, while green emission arises from the oxygen vacancy (V_o^+) states present on the surface.[33] The yellow emission is commonly observed from the oxide NWs grown by the hydrothermal method and it is attributed the hydroxyl radicals present on the surface of the NWs.[34] During chemical reaction, large amount of hydroxyl radicals are formed in the growth solution and easily attached on the surface of the NWs at the oxygen vacancy sites. Presence of large amount of hydroxyl radicals is also detected by XPS measurements as shown earlier. The integrated peak intensity of this yellow emission for different samples is consistent with the obtained content of hydroxyl component in the XPS spectra for the O 1s core level. Fig. 6(f) shows the enhancement in UV and green PL intensity (with respect to PL intensity of the undoped NWs) as a function of Al doping concentration. It is found that the PL enhancement (intensity ratio) for the UV peak first decreases up to 1% of doping and then increases for 2% of Al doping. For the green emission, it is gradually increases with the increase in Al doping concentration. However, both the UV and green emission intensities significantly reduced at a doping level of 5 at. %. The observed changes in the green emissions are consistent with the XPS spectra, which show increment in the oxygen vacancy content in the Al:ZnO NWs. It is known that the structural quality and various kinds of lattice defects significantly affect the UV emission of the ZnO nanostructures. In the present case, the gradual reduction of the UV PL intensity is caused by the deterioration of the structural quality of the Al:ZnO NWs. Here, as the doping concentration is increased, the substitution of dopant into the Zn lattice can cause strain and the oxygen in the ZnO host lattice can be shared by both Zn and Al. This will lead to neighboring disorder and local geometric disorientation in the ZnO NWs.[35,36] As a result, deterioration of the structural quality and formation of various kinds of surface defects (radiative and nonradiative) are expected. At higher doping concentration (5 at. % or more), simultaneous reduction of the UV as well as green emissions might be due to the significant enhancement of the nonradiative defects in the Al:ZnO NWs. This is consistent with the XRD analysis.

Figures 7(a)–7(c) show the room temperature PL spectra of the Al doped core-shell NWs for the samples CS1, CS2,

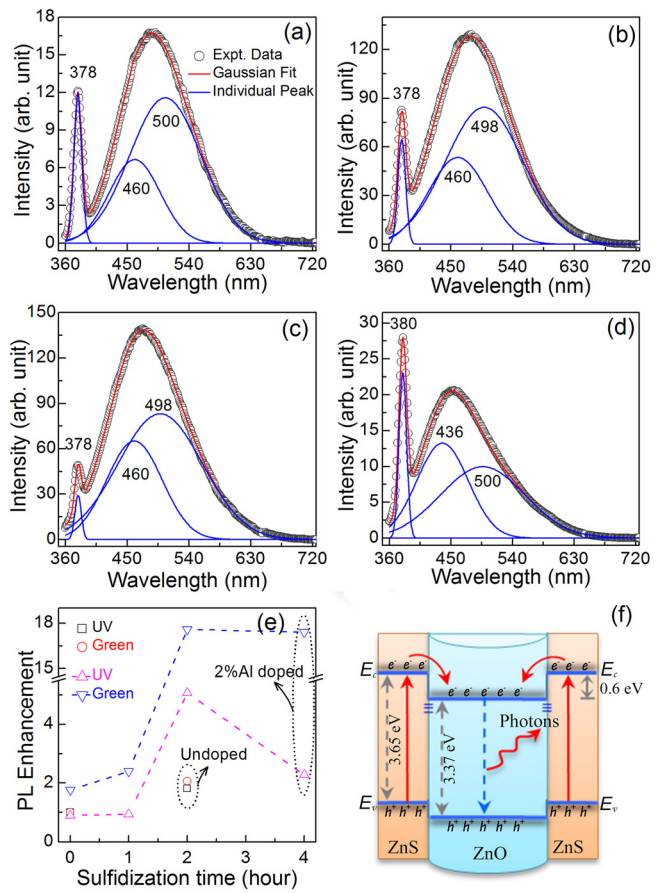

FIG. 7. Room temperature PL spectra of the Al(2 at. %):ZnO/ZnS core-shell NWs for different sulfidization time: (a) CS1, (b) CS2, and (c) CS4. (d) PL spectrum of the undoped core-shell ZnO NWs sulfidized for 2 h. (e) Variations of PL enhancement (intensity ratio) of UV and green emissions of the above core-shell NWs with respect to undoped bare ZnO NWs with sulfidization time duration. Dotted lines are shown as a viewing guidance to the data points. (f) Schematic energy band diagram of the above core-shell ZnO/ZnS NW with possible interfacial photogenerated charge transfer process.

and CS4, respectively. The PL spectra show a strong UV emission peak at 378 nm and green emission band at 500 nm. The observed PL spectra indicate significant changes in the nature of luminescence due to the formation of ZnS layer on the surface. The observed broad emission in the visible region is the superposition of two individual emissions from the core-shell NWs. Along with the green emission (from ZnO), additional peak in the blue region is observed at 460 nm. In the PL spectra, the hydroxyl radicals related yellow emission are completely suppressed, as expected. After the ZnS shell layer formation, no shift in the peak position of the UV emission observed. Note that previous reports showed a blueshift in the UV peak from ZnS coated ZnO nanospheres.[19] Figure 7(d) shows the PL spectrum of the undoped core-shell ZnO NWs sulfidized for 2 h. In this case, along with UV and green emissions, the blue emission is observed at 436 nm. This blue emission at 436 nm is associated with the ZnS shell originating from elemental sulfur vacancy or interstitial states.[37] In the Al doped core-shell NWs, the observed blue emission (at 460 nm) is shifted to the lower energy position. It is known that in case of Al doping, the impurity energy level is situated just below the conduction band of the host materials. Therefore, the observed redshift in the blue emission might be due to the involvement of the impurity (Al atoms) energy levels in the recombination process with the elemental sulfur atoms. The variations of the intensity ratio of different PL peaks (with respect to PL intensity of the undoped bare NWs) as a function of sulfidization time are shown in Fig. 7(e). The PL enhancement factors (intensity ratios) for the UV and green emissions gradually increase with the increase in ZnS shell thickness. However, after the sulfidization of 4 h, the enhancement for the green emission gets saturated and for the UV emission, it is slightly reduced. The maximum enhancement is obtained from the sample CS2, indicating the optimum thickness ($\sim$10 nm) of the ZnS shell layer. Compared with the undoped bare ZnO NWs, fivefold enhancement in the UV PL intensity is obtained from the sample CS2. As compared with the undoped ZnO/ZnS core-shell NWs, Al doped core-shell NWs show 2.8 times enhancement in UV PL intensity. Thus, the Al doped core-shell ZnO NWs show significant improvement in the UV PL intensity than the undoped core-shell ZnO NWs. Therefore, the fabricated Al doped ZnO/ZnS core-shell NWs possess very high electronic conductivity as well as sufficiently strong UV luminescence for commercial application in optoelectronic devices.

The observed improvement in the PL spectra can be explained taking the band alignment and surface modification into consideration. When the core-shell structure is excited with 325 nm light, it is expected that carriers in both the ZnO (absorption $\max^{m} \sim 367$ nm) and ZnS (absorption $\max^{m} \sim 340$ nm) get excited and excitons are created. From the absorption studies (data not shown), it is found that at 325 nm, the core-shell NWs have stronger absorption magnitude than the bare ZnO NWs. Therefore, photogenerated charge carriers are expected to be higher for the core-shell NWs than the bare NWs. It is known that the electron affinities (E_a) of ZnO and ZnS are 4.5 and 3.9 eV, respectively.[38] Therefore, an upward band offset of 0.6 eV between conduction bands of ZnO and ZnS exists in the energy band diagram of the ZnO/ZnS NWs. Then, these photogenerated energetic electrons transferred to the conduction band of ZnO through the ZnO/ZnS interface and this is schematically shown in Fig. 7(f). At the same time, the outer shell layer suppresses the tunneling of photogenerated charge carriers from the core to the newly formed surface states. This process leads to the confinement of large number of photogenerated charge carriers at the core (ZnO) resulting in strong UV PL. After substitution of sulfur atoms, the oxygen vacancies on the surface of the ZnO NW significantly modify the visible emission. In the present case, the lattice mismatch between ZnO and ZnS might be responsible for the increase of surface states at the interface causing a strong green emission. Therefore, the interfacial transfer of photogenerated electrons and confinement by suppression of tunneling by the outer ZnS shell are most likely sources of the enhanced UV PL intensity.

IV. CONCLUSIONS

We investigated the combined effects of Al doping and surface modification by ZnS shell layer on the structural, electrical, and PL properties of the ZnO NWs. A systematic investigation on effect of different concentrations of Al doping followed by formation of ZnS shell layer with different thicknesses are performed. Compared with the bare undoped ZnO NWs, a major improvement in the electronic conductivity (by two orders of magnitude) and fivefold enhancement in the UV PL intensity is obtained from the aluminum doped core-shell ZnO/ZnS NWs. As compared with the undoped ZnO/ZnS core-shell NWs, Al doped core-shell NWs show 2.8 times enhancement in UV PL intensity. The Al doped core-shell ZnO NWs show significant improvement in the UV PL than the undoped core-shell ZnO NWs. The UV PL enhancement factor could be improved further by controlling the sufidization rate and shell thickness. These results indicate that Al doping followed by ZnS shell formation on the ZnO NWs is very effective to improve electronic conductivity as well as the UV luminescence, which is promising for controlled fabrication of ZnO based optoelectronic devices.

ACKNOWLEDGMENTS

Part of the experiment was carried out under "Grant-in-Aid for Scientific Research" from Japan Society for the Promotion of Science (JSPS). S.D. would like to express sincere thanks to JSPS for awarding the postdoctoral fellowship for foreign researchers.

[1]M. Sakurai, Y. G. Wang, T. Uemura, and M. Aono, Nanotechnology **20**, 155203 (2009).
[2]Z. L. Wang and J. Song, Science **312**, 242–246 (2006).
[3]M. H. Huang, S. Mao, H. Feick, H. Yan, Y. Wu, H. Kind, E. Weber, R. Russo, and P. Yang, Science **292**, 1897–1899 (2001).
[4]N. Kumar, A. Dorfman, and J.-I. Hahm, Nanotechnology **17**, 2875–2881 (2006).
[5]L. Vj, J. Oh, A. P. Nayak, A. M. Katzenmeyer, K. H. Gilchrist, S. Grego, N. P. Kobayashi, S.-Y. Wang, A. A. Talin, N. K. Dhar, and M. S. Islam, IEEE J. Sel. Top. Quantum Electron. **17**, 1002–1032 (2011).
[6]Y. Li, F. Qian, J. Xiang, and C. M. Lieber, Mater. Today **9**, 18–27 (2006).

[7]J. S. Reparaz, F. Güell, M. R. Wagner, A. Hoffmann, A. Cornet, and J. R. Morante, Appl. Phys. Lett. **96**, 053105 (2010).
[8]C. Xu, M. Kim, J. Chun, and D. Kim, Appl. Phys. Lett. **86**, 133107 (2005).
[9]Y. Feng, W. Hou, X. Zhang, P. Lv, Y. Li, and W. Feng, J. Phys. Chem. C **115**, 3956–3961 (2011).
[10]M. S. Hammer, C. Deibel, J. Pflaum, and V. Dyakonov, Org. Electron. **11**, 1569–1577 (2010).
[11]C.-H. Hsu and D.-H. Chen, Nanotechnology **21**, 285603 (2010).
[12]P. Cheng, D. Li, Z. Yuan, P. Chen, and D. Yang, Appl. Phys. Lett. **92**, 041119 (2008).
[13]W. Park, G. Jo, W. K. Hong, J. Yoon, M. Choe, S. Lee, Y. Ji, G. Kim, Y. H. Kahng, K. Lee, D. Wang, and T. Lee, Nanotechnology **22**, 205204 (2011).
[14]T. Chen, G. Z. Xing, Z. Zhang, H. Y. Chen, and T. Wu, Nanotechnology **19**, 435711 (2008).
[15]K. W. Liu, R. Chen, G. Z. Xing, T. Wu, and H. D. Sun, Appl. Phys. Lett. **96**, 023111 (2010).
[16]W. I. Park, G.-C. Yi, M. Y. Kim, and S. J. Pennycook, Adv. Mater. **15**, 526–529 (2003).
[17]S. Dhara and P. K. Giri, J. Appl. Phys. **111**, 044320 (2012).
[18]S. Dhara and P. K. Giri, Funct. Mater. Lett. **5**, 1250021 (2012).
[19]S. K. Panda, A. Dev, and S. Chaudhuri, J. Phys. Chem. C **111**, 5039–5043 (2007).
[20]C. Liu, Z. Liu, J. Li, Y. Li, J. Han, Y. Wang, Z. Liu, and J. Ya, Microelectron. Eng. **103**, 12–16 (2013).
[21]J. Li, D. Zhao, X. Meng, Z. Zhang, J. Zhang, D. Shen, Y. Lu, and X. Fan, J. Phys. Chem. B **110**, 14685–14687 (2006).
[22]M. Y. Lu, L. Song, M. P. Lu, C. Y. Lee, L. J. Chen, and Z. L. Wang, ACS Nano **3**, 357–362 (2009).
[23]S. Dhara and P. K. Giri, J. Exp. Nanosci. **8**, 332–340 (2013).
[24]C. S. Hsiao, C. H. Peng, S. Y. Chen, and S. C. Liou, J. Vac. Sci. Technol. B **24**, 288–291 (2006).
[25]R. Viswanatha, S. Sapra, S. S. Gupta, B. Satpati, P. V. Satyam, B. N. Dev, and D. D. Sarma, J. Phys. Chem. B **108**, 6303–6310 (2004).
[26]X. Wang, P. Gao, J. Li, C. J. Summers, and Z. L. Wang, Adv. Mater. **14**, 1732–1735 (2002).
[27]Y.-C. Cheng, Appl. Surf. Sci. **258**, 604–607 (2011).
[28]F. Rueda, J. Mendialdua, A. Rodriguez, R. Casanova, Y. Barbaux, L. Gengembre, and L. Jalowiecki, J. Electron Spectrosc. Relat. Phenom. **82**, 135–143 (1996).
[29]R. Hauert, J. Patscheider, M. Tobler, and R. Zehringe, Surf. Sci. **292**, 121–129 (1993).
[30]M. Chen, X. Wang, Y. H. Yu, Z. L. Pei, X. D. Bai, C. Sun, R. F. Huang, and L. S. Wen, Appl. Surf. Sci. **158**, 134–140 (2000).
[31]S. Major, S. Kumar, M. Bhatnagar, and K. L. Chopra, Appl. Phys. Lett. **49**, 394 (1986).
[32]Y. Tanaka, H. Saito, Y. Tsutsumi, H. Doi, H. Imai, and T. Hanawa, Mater. Trans. **49**, 805–811 (2008).
[33]K. Vanheusden, W. L. Warren, C. H. Seager, D. R. Tallant, J. A. Voigt, and B. E. Gnade, J. Appl. Phys. **79**, 7983–7990 (1996).
[34]J. Qiu, X. Li, F. Zhuge, X. Gan, X. Gao, W. He, S.-J. Park, H.-K. Kim, and Y.-H. Hwang, Nanotechnology **21**, 195602 (2010).
[35]S. Dhara and P. K. Giri, Chem. Phys. Lett. **541**, 39–43 (2012).
[36]R. Kumar, N. Khare, V. Kumar, and G. L. Bhalla, Appl. Surf. Sci. **254**, 6509–6513 (2008).
[37]M. Ahmad, X. Yan, and J. Zhu, J. Phys. Chem. C **115**, 1831–1837 (2011).
[38]Y. Yang, S. Xue, S. Liu, J. Huang, and J. Shen, Appl. Phys. Lett. **69**, 377–379 (1996).